Interface localization-delocalization transition in a symmetric polymer blend: A finite-size scaling Monte Carlo study

M. Müller* and K. Binder
Institut für Physik, WA 331, Johannes Gutenberg Universität, D-55099 Mainz, Germany
(Received 21 August 2000; published 24 January 2001)

Using extensive Monte Carlo simulations, we study the phase diagram of a symmetric binary (AB) polymer blend confined into a thin film as a function of the film thickness D. The monomer-wall interactions are short ranged and antisymmetric, i.e., the left wall attracts the A component of the mixture with the same strength as the right wall does the B component, and this gives rise to a first order wetting transition in a semi-infinite geometry. The phase diagram and the crossover between different critical behaviors is explored. For large film thicknesses we find a first order interface localization-delocalization transition, and the phase diagram comprises two critical points, which are the finite film width analogies of the prewetting critical point. Using finite-size scaling techniques we locate these critical points, and present evidence of a two-dimensional Ising critical behavior. When we reduce the film width the two critical points approach the symmetry axis $\phi = 1/2$ of the phase diagram, and for $D \approx 2R_g$ we encounter a tricritical point. For an even smaller film thickness the interface localization-delocalization transition is second order, and we find a single critical point at $\phi = 1/2$. Measuring the probability distribution of the interface position, we determine the effective interaction between the wall and the interface. This effective interface potential depends on the lateral system size even away from the critical points. Its system size dependence stems from the large but finite correlation length of capillary waves. This finding gives direct evidence of a renormalization of the interface potential by capillary waves in the framework of a microscopic model.

DOI: 10.1103/PhysRevE.63.021602 PACS number(s): 05.70.Fh, 68.08.Bc, 83.80.Tc

I. INTRODUCTION

Confining a binary mixture, one can profoundly alter its miscibility behavior [1–5]. If a mixture is confined into a quasi-one-dimensional (e.g., cylindrical) pore no true phase transition occurs, unlike the prediction of the mean field theory. Fluctuations destroy long-range order, and only a pronounced maximum of the susceptibility remains in the vicinity of the unmixing transition in the bulk. In a two-dimensional system (e.g., a slitlike pore or a film) with identical surfaces a true phase transition occurs (capillary condensation) and the shift of the critical point away from its bulk value has been much investigated [6]. The confinement changes the universality class of the transition from a three-dimensional (3D) Ising critical behavior in the bulk to a 2D Ising critical behavior in the film. The latter manifests itself in much flatter binodals in a film close to the unmixing transition than in the bulk. No such change of the critical exponents is observed in mean field theory.

The phase behavior of symmetric mixtures in a thin film with antisymmetric surface interactions has attracted abiding interest recently [7–12]. The right surface attracts one species with exactly the same strength as the opposite surface attracts the other species. In contrast to capillary condensation, the phase transition does not occur close to the unmixing transition in the bulk, but rather in the vicinity of the wetting transition. Close to the unmixing transition in the bulk, enrichment layers at the surfaces are gradually built up, and an interface is stabilized in the middle of the film. In this ''soft-mode'' phase the system is laterally homogenous—no spontaneous breaking of the symmetry occurs. If the wetting transition of the semi-infinite system is of second order, one encounters a second order localization-delocalization transition slightly below the wetting transition temperature. The system phase separates laterally into regions where the interface is located close to one surface (localized state). The order parameter, i.e., the distance between the interface and the center of the film, grows continuously. This prediction of phenomenological theories was corroborated by detailed simulation studies [10,13,14], and it is also in accord with experimental findings [15,16].

If the wetting transition is of first order, and the thickness of the film not too small, mean field calculations [17,18] predict the occurrance of two critical points which correspond to the prewetting critical point of the semi-infinite system. Unlike the wetting transition, [6] the prewetting transition can produce a critical (singular) behavior in a thin film, because only the lateral correlation length diverges at the prewetting critical point; the thickness of the enrichment layers at the surfaces remains finite. The mean field treatment invokes approximations and it cannot be expected to capture the subtle interplay between 2D Ising fluctuations at the critical points, ''bulklike'' composition fluctuations, and interface fluctuations typical of the wetting transition [13]. Consequently, a detailed test of the mean field predictions via Monte Carlo simulations is certainly warranted, and elucidates the role of fluctuations. Using Monte Carlo simulations of the Ising model, Ferrenberg *et al.* also studied the interface localization-delocalization transition for the case when the wetting transition of the semi-infinite system is of first order [19]. This simulation study was centered on the dependence on the film thickness, which is a convenient parameter

*Email address: Marcus.Mueller@uni-mainz.de

to vary in experiments. However, the study was restricted to the coexistence between strictly symmetric phases, and many questions remained open.

General features of the phase behavior are shared by all binary mixtures. Here we present large scale Monte Carlo simulations aiming at investigating the phase behavior of a symmetric binary polymer blend confined between antisymmetric walls. Computationally, simulations of a polymer blend [20] are much more demanding than studying simple fluids (e.g., the Ising model), but recent mean field calculations made detailed predictions for the phase behavior of confined polymer mixtures [17,18], and serve to guide us when choosing the model parameters in the simulations. Simulating polymer blends, we can, at least in principle, control the importance of fluctuations by varying the degree of interdigitation, i.e., the chain length [18,20]. The mean field theory is expected to become accurate in the limit of infinite interdigitation. In a binary polymer blend the wetting transition occurs at much lower temperatures than the critical temperature of the unmixing transition in bulk [21]. Hence, bulklike composition fluctuations are not important in the vicinity of the wetting transition temperature, and we can isolate the effect of interface fluctuation. Moreover, these systems are also suitable candidates to examine the phase behavior experimentally. Indeed, one of the first studies of the ''soft-mode'' phase employed a binary polymer blend [15].

Our paper is broadly arranged as follows: First, we present a phenomenological description of the phase behavior in a film with antisymmetric short-ranged surface interactions. Using a standard model for the effective interface potential we calculate the phase behavior in the mean field approximation, discuss the regime of validity of the mean field approach, and consider the crossover between the different critical behaviors. Second, we briefly describe our coarse grained lattice model for a binary polymer mixture. Then we present our Monte Carlo results: We obtain the phase diagram for film thicknesses ranging from $D=1.1R_g$ to $7R_g$, where R_g denotes the radius of gyration of the polymer chains, investigate the critical behavior and present evidence that interface fluctuations renormalize the effective interface potential. We close with a comparison of the phase diagram to the behavior of the bulk and of films with symmetric boundary conditions.

II. BACKGROUND

Rather than describing the configuration of the system by a detailed composition profile across the film, much qualitative insight into the thermodynamics can be deduced from the effective interface potential. Below the bulk critical temperature, enrichment layers of the prefered components form at the surfaces and stabilize an AB interface which runs parallel to the walls. The effective interface potential $g_{\mathrm{wall}}(l)$ describes the free energy per unit area as a function of the distance l between this AB interface and a wall. In the case of short-ranged forces between the monomers and the walls, the interface profile becomes distorted in the vicinity of the walls, and this gives rise to an interaction which decays exponentially as a function of the distance l between the AB interface and a single wall:

$$g_{\mathrm{wall}}(l)=a\exp(-\lambda l)-b\exp(-2\lambda l)+c\exp(-3\lambda l). \tag{1}$$

This expression retains only the lowest powers of $\exp(-\lambda l)$, which are necessary to bring about a first order wetting transition of the semi-infinite system. The coefficient a is explicitly temperature dependent, while the temperature dependence of b and c is neglected. $c>0$ is assumed throughout the discussion. All coefficients are of the same magnitude as the interfacial tension σ between the coexisting bulk phases. For polymer blends this quantity scales with chain length N and monomer number density ρ like $\sqrt{\bar{N}}/R_g^2$. $\bar{N}=(\rho R_g^3/N)^2$ measures the degree of interdigitation. $1/\lambda$ denotes the spatial range of the interactions, and it is of the order R_g. $b<0$ gives rise to a second order wetting transition at $a=0$, and $b=0$ to a tricritical transition. For $b>0$ one encounters a first order wetting transition at $a_{\mathrm{wet}}=b^2/4c$, where the thickness of the enrichment layer jumps discontinuously from $l_-=1/\lambda\ln(2c/b)$ to a macroscopic value [18]. The wetting spinodals take the values $a>0$ (from the wet phase) and $a<b^2/3c$ (from the nonwet phase). The concomitant prewetting line terminates at the prewetting critical point $a_{\mathrm{pwc}}=16a_{\mathrm{wet}}/9$ and $l_{\mathrm{pwc}}=1/\lambda\ln(9c/2b)$.

We approximate the effective interface potential in a film to be the linear superposition of the interactions originating at each wall and analyze the behavior. Self-consistent-field calculations [18] lend support to this approximation. The interface potential in a film of thickness D takes the form

$$\begin{aligned} g(l)&=g_{\mathrm{wall}}(l)+g_{\mathrm{wall}}(D-l)-2g_{\mathrm{wall}}(D/2)\\ &=2a\exp(-\lambda D/2)(\cosh(\lambda[l-D/2])-1)\\ &\quad-2b\exp(-\lambda D)(\cosh(2\lambda[l-D/2])-1)\\ &\quad+2c\exp(-3\lambda D/2)(\cosh(3\lambda[l-D/2])-1). \end{aligned} \tag{2}$$

In general, the phase boundaries depend on the variables a/c, b/c, and λD. If we proceeded as in Ref. [13] by expanding the cosh in powers of $[l-D/2]$, further analysis would be rather cumbersome. A more transparent procedure employs the variable

$$\begin{aligned} \tilde{m}^2&=2\exp(-\lambda D/2)(\cosh(\lambda[l-D/2])-1)\\ &=(\exp(-\lambda D/4)\lambda[l-D/2])^2+\text{higher orders of }[l-D/2] \end{aligned} \tag{3}$$

to rewrite the interface potential in the form

$$g(l)=c[\tilde{m}^2(\tilde{m}^2-r)^2+t\tilde{m}^2]$$

with

$$r=\frac{b-6c\exp(-\lambda D/2)}{2c}$$

and

$$t=\frac{a-a_{\rm wet}-b\,\exp(-\lambda D/2)}{c}. \tag{4}$$

The qualitative form of the effective interface potential was inferred previously on the basis of a Landau expansion [18]. Here it is derived explicitly from the standard form of the interface potential [Eq. (1)] for a first order wetting transition in a semi-infinite system. Negative values of r correspond to second order localization-delocalization transitions, $r=0$ to a tricritical one, and positive values of r give rise to first order transitions. t measures the distance from the tricritical transition temperature (for $r\leqslant 0$), and $t=0$ denotes the triple temperature in the case of a first order interface localization-delocalization transition (see below). For $r\leqslant 0$ the phase boundaries depend only on the two parameter combinations r and t. In these variables the limit $\lambda D\to\infty$ is particularly transparent: $cr\to b/2$, $ct\to a-a_{\rm wet}$, and $\tilde{m}\to\exp(-\lambda l)$.

A. $r\leqslant 0$: Second order and tricritical interface localization-delocalization transition

A second order interface localization-delocalization transition (i.e., $r<0$) will occur either if the wetting transition is second order (i.e., $b<0$) or if the wetting transition is first order but the film thickness D small enough to comply with $0<b<6c\,\exp(-\lambda D/2)$. This behavior is in accord with previous findings [9,19,18], and we shall corroborate this further by our present simulations. Since the coexisting phases are symmetric with respect to exchanging l and $D-l$, phase coexistence occurs at $\Delta\mu_{\rm coex}\equiv 0$ or $\partial g/\partial l=(\partial g/\partial\tilde{m})(d\tilde{m}/dl)=0$. From this condition, for the binodals we obtain

$$\tilde{m}^2=\frac{2|r|}{3}\left(\sqrt{1+\frac{3}{4r^2}\Delta t}-1\right)\to\begin{cases}\Delta t/4|r| & \text{for } \Delta t\ll r^2 \quad (2\text{DMF})\\ \sqrt{\Delta t/3} & \text{for } \Delta t\gg r^2 \quad (2\text{DTMF}).\end{cases} \tag{5}$$

The critical temperature is given by $t_c=-r^2$, and $\Delta t=t_c-t$ denotes the distance from the critical temperature at fixed r. For $r<0$ the binodals at the critical point open with the mean field exponent $\beta_{\rm 2DMF}=1/2$. This corresponds to mean field critical behavior (2DMF) of a system with a single scalar order parameter, i.e., $m=[l/D-1/2]$. At larger distance the order parameter grows like $m\sim(\Delta t)^{\beta_{\rm 2DTMF}}$ with $\beta_{\rm 2DTMF}=1/4$. The latter exponent is characteristic of the mean field behavior at a tricritical point (2DTMF). The crossover between mean field critical and tricritical behaviors occurs around $|\Delta t_{\rm cross}|\sim r^2$. As we decrease the magnitude of $r\to 0$ we approach the tricritical point and the regime where mean field critical behavior is observable shrinks. At the tricritical point only the tricritical regime (2DTMF) exists, i.e., $\Delta t_{\rm cross}=0$, and the binodals take the particularly simple form $\tilde{m}=(\Delta t/3)^{1/4}$. The crossover in the binodals for $r=-0.4$ is illustrated in the inset of Fig. 1(a).

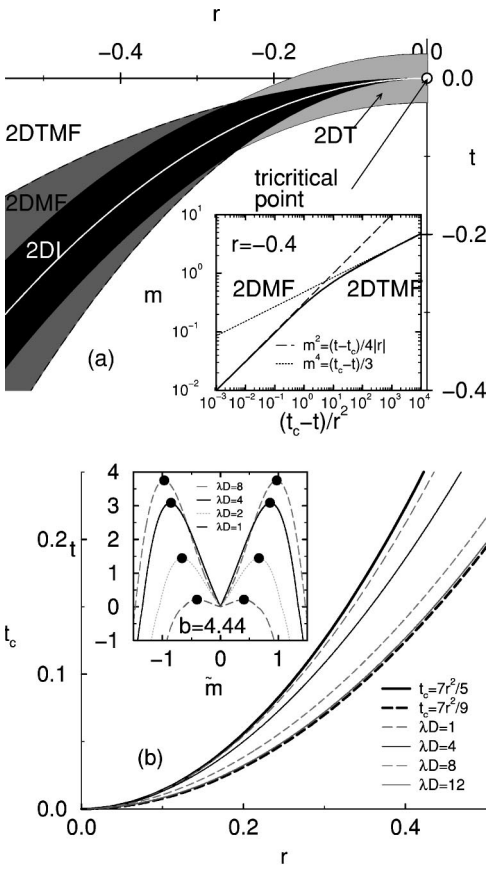

FIG. 1. (a) Illustration of the different regimes for a second order and tricritical transition. 2DTMF: mean field tricritical behavior; 2DMF: mean field critical behavior; 2DI: two-dimensional Ising critical behavior; 2DT: two-dimensional tricritical behavior. The inset shows the temperature dependence of the order parameter $\tilde{m}$ for $r=-0.4$ as calculated within mean field theory [see Eq. (5)]. For $t_c-t\ll 16r^2/3$, 2DMF behavior is found, while 2DTMF behavior is observed at larger distances from the critical point. (b) Dependence of the critical temperature t_c on the distance r from the tricritical point. The curves correspond to different values of λD, as indicated in the key. Thick lines, which bracket the behavior, correspond to $t_c=7r^2/5$ (valid for small r) and $t_c=7r^2/9$ (valid in the limit $\lambda D\to\infty$). The inset presents the binodals at fixed strength $b=4.44$ of the wetting transition of the individual surface, and several values of λD as indicated in the key. For the choice of parameter $b/c=4.44>3\,\exp(-\lambda D/2)$ (and, hence, $r>0$), there are two critical points for all values of the film thickness.

Of course, the above considerations neglect fluctuations and the behavior close to the transition is governed by Ising critical exponents and two-dimensional tricritical exponents, respectively. The crossover between Ising critical behavior (2DI) and tricritical behavior (2DT) occurs at $|\Delta t_{\rm cross}|\sim r^{1/\phi_{\rm cross}}$, where the crossover critical exponent is not 1/2 (as for the crossover between the mean field regimes) but rather 4/9 [22–24]. Following Ref. [13] we calculate the critical amplitudes, and estimate the location of the crossover between mean field critical behavior and the region where fluc-

tuations dominate the qualitative behavior. For small values of the order parameter $m=[l/D-1/2]$ we approximate $m \approx \tilde{m}\exp(\lambda D/4)/(\lambda D)$, and obtain, for the mean field critical amplitudes,

$$\hat{B}_{\mathrm{2DMF}}=\frac{\exp(\lambda D/4)}{2\sqrt{|r|}\lambda D} \quad \text{and} \quad \hat{B}_{\mathrm{2DTMF}}=\frac{\exp(\lambda D/4)}{3^{1/4}\lambda D}. \tag{6}$$

The susceptibility of the order parameter above the critical temperature is related to the inverse curvature of the interface potential in the middle of the film $1/\chi D^2=(\partial^2 g/\partial l^2)_{|l=D/2}$. Using Eq. (4), for critical and tricritical mean field transitions we obtain

$$\chi=\frac{1}{2c(\lambda D)^2}\exp(\lambda D/2)\Delta t^{-1}$$

and

$$\hat{C}^{+}_{\mathrm{MF}}=\frac{1}{2c(\lambda D)^2}\exp(\lambda D/2), \quad \gamma_{\mathrm{MF}}=1. \tag{7}$$

The ratio $\hat{C}^{+}_{\mathrm{MF}}/\hat{C}^{-}_{\mathrm{MF}}$ of the critical amplitudes above and below the critical point is universal, and takes a mean field value 2 at the critical point and 4 at the tricritical point. At the transition the correlation length $\xi_{\parallel}$ diverges. This lateral length is associated with fluctuations of the local interface position, i.e., capillary waves. In mean field approximation the parallel correlation length takes the form

$$\xi_{\parallel}=\left(\frac{1}{\sigma}\frac{\partial^2 g}{\partial l^2}\right)^{-1/2}=\sqrt{\sigma D^2\chi}$$

hence

$$\hat{\xi}^{+}_{\mathrm{MF}}=\frac{\sqrt{\sigma}}{\lambda\sqrt{2c}}\exp(\lambda D/4), \quad \gamma_{\mathrm{MF}}=1/2, \tag{8}$$

and $\hat{\xi}^{+}_{\mathrm{MF}}/\hat{\xi}^{-}_{\mathrm{MF}}=\sqrt{2}$ and 2, respectively.

Knowing the critical amplitudes we can estimate the importance of fluctuations via the Ginzburg criterium [25]. As it is well known, mean field theory is self-consistent if the fluctuations of the order parameter in a volume of linear dimension $\xi_{\parallel}$ are small in comparison to the mean value of the order parameter. For our quasi-two-dimensional system $(d=2)$, we obtain

$$\frac{\chi}{\xi_{\parallel}^{d}} \overset{!}{\ll} m^2 \Rightarrow \left(\frac{c^{1-2/d}\lambda^2}{\sigma}\right)^{d/2}\exp(-d\lambda D/4)$$
$$\overset{!}{\ll} \begin{cases} \dfrac{1}{|r|}\Delta t^{(4-d)/2} & \text{for } r<0 \quad \text{second order} \\ \Delta t^{(3-d)/2} & \text{for } r=0 \quad \text{tricritical.} \end{cases} \tag{9}$$

This result is as expected: For a second order interface localization-delocalization transition in our quasi-two-dimensional system we obtain $\Delta t \ll G i_{\mathrm{2DI}} \sim |r|\exp(-\lambda D/2)/\sqrt{\bar{N}}$, in accord with Ref. [13], while we obtain $\Delta t \ll G i_{\mathrm{2DT}} \sim \exp(-\lambda D)/\bar{N}$ upon approaching the tricritical point. For bulk $(d=3)$ tricritical phenomena Landau theory is marginally correct.

Combining the above results we find the following behavior upon approaching the critical temperature: Far away from the tricritical point, i.e., $r \gg \exp(-\lambda D/2)/\sqrt{\bar{N}}$, we find a mean field tricritical behavior (2DTMF) for $\Delta t \gg r^2$, a mean field critical behavior (2DMD) for $r^2 \ll \Delta t \ll |r|\exp(-\lambda D/2)$, and finally a two-dimensional Ising critical behavior (2DI) for $|r|\exp(-\lambda D/2) \gg \Delta t$. Closer to the tricritical point, i.e., $r \ll \exp(-\lambda D/2)/\sqrt{\bar{N}}$, we find a mean field tricritical behavior (2DTMF) for $\Delta t \gg \exp(-\lambda D/4)$, a two-dimensional tricritical behavior (2DT) for $\exp(-\lambda D/4) \ll \Delta t \ll C r^{1/\phi_{\mathrm{cross}}}$, and an Ising critical behavior (2DI) for $C r^{1/\phi_{\mathrm{cross}}} \gg \Delta t$. The prefactor C must be chosen such that all crossover lines (2DI$\leftrightarrow$2DT, 2DT$\leftrightarrow$2DTMF, 2DTMF$\leftrightarrow$2DMF, and 2DMF$\leftrightarrow$2DI) intersect at a common point. This yields $C \sim [\bar{N}\exp(\lambda D)]^{-1+1/2\phi_{\mathrm{cross}}}$. Of course, the term ''crossover line'' is not meant as a sharp division between different behaviors, but should rather be understood as the center of a smooth crossover region. Likewise, the above constant C may involve a constant of order unity which has been suppressed for simplicity. The two different sequences can be clearly distinguished in the Monte Carlo simulations, because the probability distribution of the order parameter exhibits a three peak structure [36] only close to the tricritical point (2DT). We shall use this property to analyze our Monte

TABLE I. Compilation of the boundaries of the different regimes in the vicinity of the tricritical point and the correlation lengths at the crossover. The latter quantity gives an estimate of the system size required to observe the crossover in the Monte Carlo simulations.

Crossovers	$\lvert\Delta t_{\mathrm{cross}}\rvert$	ξ_{cross}/R_g
2DT $\leftrightarrow$ 2DI	$(\bar{N}\exp(\lambda D))^{-1+1/2\phi_{\mathrm{cross}}} r^{1/\phi_{\mathrm{cross}}}$	$\exp(\lambda D(3/4-\nu_{\mathrm{tri}}/2\phi_{\mathrm{cross}}))\bar{N}^{1/2-\nu_{\mathrm{tri}}/2\phi_{\mathrm{cross}}} r^{-\nu_{\mathrm{tri}}/\phi_{\mathrm{cross}}}$
2DI $\leftrightarrow$ 2DMF	$\lvert r\rvert\bar{N}^{-1/2}\exp(-\lambda D/2)$	$\lvert r\rvert^{-1/2}\bar{N}^{1/4}\exp(\lambda D/2)$
2DMF $\leftrightarrow$ 2DTMF	r^2	$\lvert r\rvert^{-1}\exp(\lambda D/4)$
2DTMF $\leftrightarrow$ 2DT	$\bar{N}^{-1}\exp(-\lambda D)$	$\bar{N}^{1/2}\exp(3\lambda D/4)$

Carlo (MC) simulations. The anticipated behavior is summarized in Fig. 1(a).

In the Monte Carlo simulation this rich crossover scenario is further complicated by finite-size rounding. The Monte Carlo results are subjected to pronounced finite-size effects whenever the correlation length becomes of the order of the lateral system size. In the mean field regime the correlation length scales like $\xi_\parallel \sim R_g \exp(\lambda D/4)\Delta t^{-1/2}$. Knowing the Ginzburg number for the crossover from 2DMF to 2DI behavior, we estimate the correlation length in the Ising critical regime [13],

$$\xi_\parallel \sim R_g \exp(\lambda D/4)\Delta t^{-1/2}\tilde{f}(\Delta t/Gi_{\rm 2DI}) \rightarrow \begin{cases} R_g \exp(\lambda D/4)\Delta t^{-1/2} & \text{for } \Delta t \gg Gi_{\rm 2DI} \\ R_g |r|^{1/2}\overline{N}^{-1/4}\Delta t^{-1} & \text{for } \Delta t \ll Gi_{\rm 2DI}, \end{cases} \tag{10}$$

where we have assumed that the scaling function $\tilde{f}$ assumes a power law behavior for small and large arguments, and we have used the value $\nu_{\rm 2DI}=1$ appropriate for the divergence of the correlation length in the 2DI regime. Similarly, we determine the correlation length in the 2DT regime:

$$\xi_\parallel \sim R_g \exp(\lambda D/4)\Delta t^{-1/2}\tilde{f}(\Delta t/Gi_{\rm 2DT}) \rightarrow \begin{cases} R_g \exp(\lambda D/4)\Delta t^{-1/2} & \text{for } \Delta t \gg Gi_{\rm 2DT} \\ R_g \exp(\lambda D(3/4-\nu_{\rm tri}))\overline{N}^{1/2-\nu_{\rm tri}}\Delta t^{-\nu_{\rm tri}} & \text{for } \Delta t \ll Gi_{\rm 2DT}. \end{cases} \tag{11}$$

$\nu_{\rm tri}=5/9$ denotes the exponent of the correlation length in the 2DT universality class [22–24]. The correlation lengths at the various crossovers are compiled in Table I. The largest correlation length occurs at the crossover from 2DT to 2DI behavior:

$$\xi_\parallel^{2DT\leftrightarrow 2DI} \sim R_g \exp[\lambda D(3/4-\nu_{\rm tri}/2\phi_{\rm cross})] \times \overline{N}^{1/2-\nu_{\rm tri}/2\phi_{\rm cross}} |r|^{-\nu_{\rm tri}/\phi_{\rm cross}}. \tag{12}$$

In order to observe the true Ising critical behavior for negative values of r, the system size L has to exceed this correlation length. In the vicinity of the tricritical point (i.e., for small negative values of r) this requirement is very difficult to be met in computer simulations.

B. $r>0$: First order interface localization-delocalization transition

For positive values of r the interface potential exhibits a three valley structure. The three minima at $\tilde{m}=\pm\sqrt{r}$ and $\tilde{m}=0$ have equal free energy at $t=0$. This corresponds to the triple point. At lower temperatures an A-rich phase coexist with a B-rich phase, and since the two phases are symmetrical the coexistence occurs at $\Delta\mu_{\rm coex}=0$. The binodals below the triple point take the form

$$\tilde{m}=\pm\sqrt{\frac{2r}{3}+\sqrt{\frac{r^2}{9}-\frac{t}{3}}} \quad \text{for } t<0, \quad r>0. \tag{13}$$

Above the triple temperature $t>0$ there are two two phase coexistence regions symmetrically located around $\tilde{m}=0$. These phase coexistences terminate at two critical points. Since the coexisting phases correspond to thick and thin enrichment layers of the prefered phase at each wall, there is no symmetry between the coexisting phases, and the exchange potential $\Delta\mu_{\rm coex}$ at coexistence differs from zero. Unfortunately, the phase boundaries for $t>0$ and $r>0$ depend not only on r and t but also on λD explicitly, and we have determined them numerically. The dependence of the critical temperature t_c on r for several values of λD is presented in Fig. 1(b). The coexistence curve for $b/c=4.44$ and various values of λD are presented in the inset of Fig. 1(b). As the film thickness is decreased the critical temperature decreases, and the critical points move closer to the symmetry axis of the phase diagram. They are determined by the condition

$$\frac{\partial^2 g}{\partial l^2}=\frac{\partial^3 g}{\partial l^3}=0 \quad \text{at } t=t_c \quad \text{and } \tilde{m}=\tilde{m}_c. \tag{14}$$

In two limiting cases a simple behavior emerges.

(i) If $|\lambda(l-D/2)|\ll 1$ we can replace the derivative with respect to l by derivatives with respect to $\tilde{m}$ and, obtain [18] $t_c=7r^2/5$ and $\tilde{m}_c=\pm\sqrt{2r/5}$. This approximation holds for $r\ll\exp(-\lambda D/2)$. Expanding g in powers of $\delta\tilde{m}=\tilde{m}-\tilde{m}_c$ we obtain (omitting an irrelevant term linear in $\delta\tilde{m}$)

$$g(\tilde{m})\approx c(t_c-t)\delta\tilde{m}^2+4rc\,\delta\tilde{m}^4+\frac{7c}{3}\delta\tilde{m}^5+c\,\delta\tilde{m}^6. \tag{15}$$

This allows us to calculate the binodals in the vicinity of the critical points, the susceptibility, and the parallel correlation length. The presence of a fifth order term in $\delta\tilde{m}$ in expansion (15) is a manifestation of the fact that the phase boundaries of the prewetting transitions are not symmetric around $\tilde{m}_c$. This lack of symmetry is also evident from the numerical results in Fig. 1(b) (inset). The critical amplitudes scale in the same way with r, $\overline{N}$, and λD as for $r<0$. In particular we find, for the crossover between 2DMF and 2DI behaviors, $Gi_{\rm 2DI}\sim|r|\exp(-\lambda D/2)/\sqrt{\overline{N}}$.

(ii) In the limit of large film thickness $\lambda D\rightarrow\infty$, the critical point tends toward a prewetting critical point at $t_c\rightarrow t_{\rm pwc}=7r^2/9$. In this limit confinement effects are negligible, and the coexistence curves in the vicinity of the critical points

correspond to the prewetting lines at the corresponding surfaces. We expect the same critical behavior as at the prewetting critical point. In this case the Ginzburg number does not depend on the film thickness. For $\lambda D \to \infty$ we employ the interface potential at a single wall, and for the validity of the mean field description we find

$$\frac{a - a_{\mathrm{pwc}}}{a_{\mathrm{pwc}}} \gg \frac{\lambda^2}{\sigma} \sim \bar{N}^{-1/2} \sim Gi_{\mathrm{2DI}} \quad \text{for } r > 0, \quad \lambda D \to \infty. \tag{16}$$

III. BOND FLUCTUATION MODEL AND SIMULATION TECHNIQUE

Modeling polymeric composites from the chemical details of the macromolecular repeat units to the morphology of the phase separated blend within a single model is not feasible today, even with state-of-the-art supercomputers. However, there is ample evidence that by a careful choice of simulation and analysis techniques, coarse grained models of flexible polymers—like the bond fluctuation model [20,26]—provide useful insights into the universal polymeric features. In the framework of the bond fluctuation model each effective monomer blocks a cube of eight neighboring sites from further occupancy on a simple cubic lattice in three dimensions. Effective monomers are connected by bond vectors of length 2, $\sqrt{5}$, $\sqrt{6}$, 3, or $\sqrt{10}$ in units of the lattice spacing. The bond vectors are chosen such that the excluded volume condition guarantees that chains do not cross during their motion [27]. Each effective bond represents a group of $n \approx 3-5$ subsequent C-C bonds along the backbone of the chain [28]. Hence the chain length $N=32$ employed in the present simulations corresponds to a degree of polymerization of 100–150 in a real polymer. If we increased the chain length N, the mean field theories would yield a better description of the equilibrium thermodynamics (self-consistent-field theory is believed to be quantitatively accurate in the limit $N \to \infty$), but the length scale of the ordering phenomena would be larger. Hence our choice of N is a compromise determined by the computational resources. The statistical segment length b in the relation for the radius of gyration $R_g = b\sqrt{N/6}$ is $b = 3.05$ (i.e., $R_g \approx 7$ for $N=32$).

We study thin films of geometry $L \times L \times D$. Periodic boundary conditions are applied in the two lateral directions, while there are hard impenetrable walls at $z=0$ and $z=D+1$, modeling a film of thickness D. The average number density in the film is $\rho_0 = 1/16$, i.e., half of the lattice sites are occupied by corners of monomers. This density corresponds to a melt or concentrated solution. The density profile of occupied lattice sites, normalized by the bulk value, is presented in Fig. 2 for film thicknesses $D=24$ and 48. For this choice of temperature and monomer-wall interaction an interface is stabilized in the center of the film. Due to the extended shape of the monomers and the compressibility of the fluid there are packing effects at the walls [21]. Overall the walls are repulsive, and the monomer density is slightly reduced in the boundary region. The spatial extension of this region is independent of the film thickness. Moreover, the density is reduced at the center of the interface as to reduce

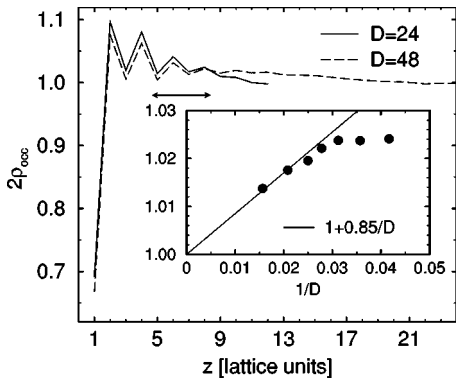

FIG. 2. Density of blocked lattice sites normalized by the bulk value as a function of the distance from the wall at $\epsilon = 0.06$ and $\epsilon_w = 0.16$ for film thicknesses $D=24$ and 48. Note the strong packing effects at the wall for $z \leqslant 5$. For these parameters an interface is stabilized at the center of the film. The position of the interface fluctuates in the interval $R_g \approx 7 < z < D - R_g$ (cf. Fig. 6) The inset presents the normalized density averaged over layers 5–8. This region is marked by the arrow in the main panel.

the energetically unfavorable contacts between unlike species [29]. Both effects are not incorporated into the mean field calculations [17,18] and cause the density in the bulk-like region of the film to be slightly larger for thinner films than for thicker ones. In the following we employ the density of occupied lattice sites in the layers $5 \leqslant z \leqslant 8$ as a measure of the density of the film. For large D the data are compatible with a behavior of the form $\rho = \rho_0(1 + 0.85/D)$. The film thickness ranges from $D = 12 \approx 1.7R_g$ to $D = 48 \approx 7R_g$, and we vary the lateral extension over a wide range $48 \leqslant L \leqslant 264$ to analyze finite-size effects. In the two layers nearest to the walls, monomers experience a monomer-wall interaction. An A monomer is attracted by the left wall and repelled by the right wall; the interaction between B monomers and the walls is exactly opposite. Each monomer-wall interaction changes the energy by an amount $\epsilon_w = 0.16$ in units of $k_B T$. For these parameters the wetting transition and the phase diagram of a blend confined between symmetric walls has been investigated previously [21].

Binary interactions between monomers are catered for by a short ranged square well potential $\epsilon \equiv -\epsilon_{AA} = -\epsilon_{BB} = \epsilon_{AB} \equiv 1/k_B T$, which is extended up to a distance $\sqrt{6}$. The phase separation is brought about by the repulsion between the unlike species. The Flory-Huggins parameter is $\chi = 2z_{\mathrm{eff}}\epsilon$, where $z_{\mathrm{eff}} \approx 2.65$ denotes the effective coordination number in the bulk [30,20] at $\rho_0 = 1/16$. For $\epsilon_w = 0.16$ previous simulations find a strong first order wetting transition at $T_{\mathrm{wet}} = 1/\epsilon_{\mathrm{wet}} = 14.1(7)$ [21]. This value corresponds to $\chi N \approx 12$, which is well inside the strong segregation limit.

The polymer conformations are updated via a combination of random monomer displacements and slithering snake-like movements. The latter relax the chain conformations about a factor of N faster than the local displacements [30]. We work in the semi-grand-canonical ensemble [31], i.e., we control the temperature $T \equiv 1/\epsilon$ and the exchange potential $\Delta\mu$ between the two species, and the concentration fluctuates. This semi-grand-canonical ensemble is realized in

Monte Carlo simulations via switching the polymer identity $A \rightleftharpoons B$ at a fixed chain conformation. Different Monte Carlo moves are applied in the ratio slithering snake:local displacements:semi-grand-canonical identity switches, which is 12:4:1. During production runs, we record all 150 slithering snake steps—the composition, energy, and surface energy—and obtained the joint probability distribution in the form of a histogram. We use semi-grand-canonical identity switches in conjunction with a reweighting scheme [29,32], i.e., to the Hamiltonian of the system we add a reweighting function $\mathcal{H}_{\rm rw}=\mathcal{H}_{\rm orig}+W(\phi)$, which depends only on the overall composition $\phi=n^A_{\rm poly}/(n^A_{\rm poly}+n^B_{\rm poly})$. $n^A_{\rm poly}$ and $n^B_{\rm poly}$ denote the number of A and B polymers in the simulation cell, respectively. The choice $W(\phi)\approx-\ln P(\phi)$, where $P(\phi)$ denotes the probability distribution of the composition in the semi-grand-canonical ensemble, encourages the system to explore configurations in which both phases coexist in the simulation cell. Otherwise these configurations would be severely suppressed due to the free energy cost of interfaces. In the framework of this reweighting scheme the system often ''tunnels'' from one phase to the other, and this allows us to locate the phase coexistence accurately and measure the free energy of the mixture as a function of the composition ϕ. Use of histogram extrapolation technique [33] permits histograms obtained at one set of model parameters to be reweighted to yield estimates appropriate to another set of model parameters. We employ this analysis technique to obtain estimates for the reweighting function $W(\phi)$.

IV. RESULTS

First, we locate the critical points of the phase diagrams. For a very small film thickness we find a second order localization-delocalization transition even though the wetting transition is of first order. Swift *et al.* predicted this behavior in the framework of a square gradient theory [9], and such a behavior is also borne out in our self-consistent-field calculations for polymer blends [17,18] and simulations of the Ising model [19]. Upon increasing the film thickness we encounter a nearly tricritical transition. A truly tricritical transition cannot be achieved by tuning the film thickness only, because of the discreteness of the lattice, but it could be brought about by varying the monomer-wall interaction. In an experiment using real materials, of course, the film thickness can be varied continuously, and a truly tricritical transition is in principle always accessible. For an even larger film thickness the interface localization-delocalization transition is first order and we find two critical points at $\phi\neq 1/2$.

Second, we locate the triple line for the two largest values of the film thicknesses, and discuss how capillary waves lead to a strong dependence of the effective interface potential on the lateral system size.

Third, we detail our results on the thickness dependence of the phase diagram, and relate our findings to the binodals of the bulk and the mixture confined into a film with symmetric boundaries.

A. Critical points

1. $D=8\approx 1.1R_g$ and $D=12\approx 1.7R_g$: second order interface localization-delocalization transition

For film thicknesses which are comparable to the radius of gyration of the molecules, the effective interface potentials originating from the two surfaces strongly interfere. This might change the order of the interface localization-delocalization transition from first to second. In this case, a single critical point occurs on the symmetry axis $\phi=1/2$ of the phase diagram. The transition is thought to belong to the 2D Ising universality class. In Fig. 3(a) we present the probability distribution of the composition for various inverse temperatures ϵ, film thickness $D=8$, and lateral film extension $L=80$. Upon increasing the monomer-monomer interaction ϵ the probability distribution $P(\phi)$ changes from single peaked to bimodal, which indicates that a phase transition occurs in this temperature range. No signature of the trimodal distribution occurs, and hence we conclude that the system is far away from the tricritical point, i.e., $|r|>\exp(-\lambda D/2)/\sqrt{N}$. In this case, we expect a crossover from 2DMF to 2DI behavior.

Along the coexistence curve $\Delta\mu=0$ and its extension to higher temperatures we use the cumulant intersection method to locate the critical point [35]. In the vicinity of the critical point the probability distribution of the order parameter $m=\phi-\phi_{\rm coex}=\phi-1/2$ scales to leading order like [35]

$$P(m,L,t)\sim L^{\beta/\nu}P^{\star}(L^{\beta/\nu}m,L^{-1/\nu}t), \tag{17}$$

where $t=(\epsilon_c-\epsilon)/\epsilon_c$ denotes the distance from the critical point along the coexistence curve, and β and ν are the critical exponents of the order parameter and the correlation length. $P^{\star}$ is characteristic of the universality class, and was obtained from simulations of the Ising model [34] at the critical temperature $t=0$. Cumulants of the form $\langle m^2\rangle/\langle|m|\rangle^2$ are expected to exhibit a common intersection point for different system sizes L at the critical temperature [35]. The value of the cumulant at the intersection point is universal. Our simulation data are presented in panel (b) and exhibit some corrections to scaling due to the crossover 2DMF to 2DI behavior. Similar corrections were observed in simulations of a second order interface localization-delocalization transition in the Ising model [13]. From the intersection points of neighboring system sizes and from the intersection of the cumulant with the universal value of the Ising model, we estimate the critical temperature to be $\epsilon_c=0.0520(5)$.

In the inset of Fig. 3(b) we show the probability distribution normalized to unit variance and norm at our estimate of the critical temperature $\epsilon_c=0.052$, and compare the distribution to the universal scaling curve of the 2D Ising universality class. The probability distributions for the smaller system sizes are slightly broader than the universal scaling curve, but the deviations decrease as we increase the system size.

The simulation data for $D=12$ are presented in Figs. 3(c) and 3(d). As we lower the temperature the probability distribution of the composition for $L=48$ changes from single peaked to bimodal. At intermediate values of ϵ, however, a

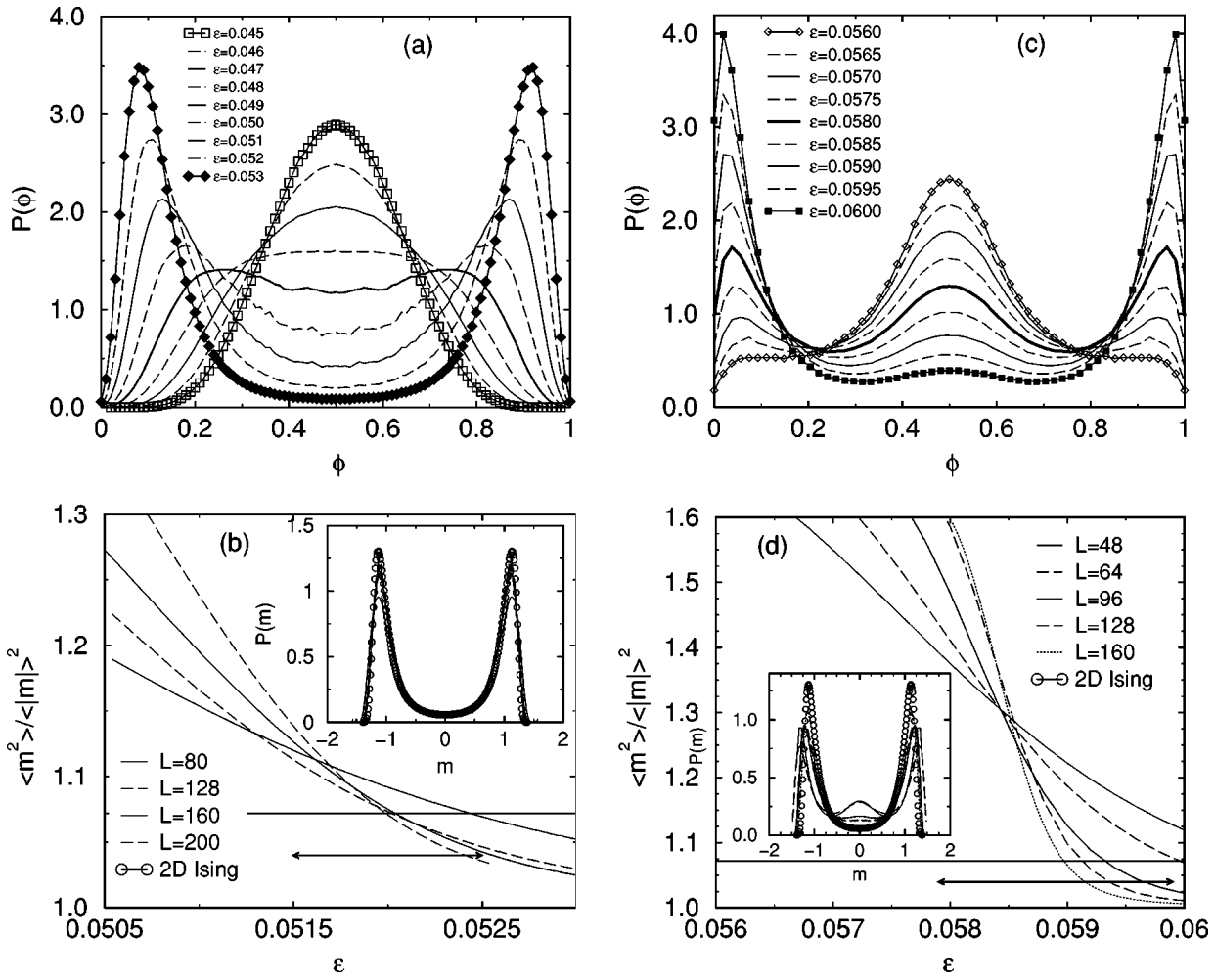

FIG. 3. (a) Probability distribution of the composition for system sizes $D=8$ and $L=80$. The inverse temperatures are indicated in the key. Histogram reweighting has been applied to extrapolate the data along the coexistence curve. The shape of the distribution function changes from single peaked to bimodal, but there is no indication of a third peak at $\phi=1/2$. (b) Cumulant ratio $\langle m^2\rangle/\langle|m|\rangle^2$ along the coexistence curve $\Delta\mu=0$ for film thickness $D=8$ and various lateral extensions L, as indicated in the key. In the finite size scaling limit $L\to\infty$, $t\equiv(\epsilon-\epsilon_c)/\epsilon_c\to 0$, and Lt finite, the cumulant intersection should occur at the value $\langle m^2\rangle/\langle|m|\rangle^2=1.072$, highlighted by the horizontal straight line. Our estimate of the critical temperature $\epsilon_c=0.0520(5)$ is indicated by the double arrow. The inset shows the distribution function of the order parameter—scaled to unit norm and variance—at our estimate of the critical temperature, and compares the MC results to the universal distribution of the 2D Ising universality class. (c) Same as (a), but for system sizes $D=12$ and $L=48$. Note that there is a broad range of ϵ where the distribution has three peaks, unlike the Ising model. This indicates the vicinity of the tricritical point. (d) Cumulant ratio $\langle m^2\rangle/\langle|m|\rangle^2$ for film thickness $D=12$ and various lateral extensions L, as indicated in the key. Our estimate of the critical temperature $\epsilon_c=0.0589(10)$ is indicated by the double arrow. The inset shows the distribution function of the order parameter at our estimate of the critical temperature, and compares the MC data to the universal distribution of the 2D Ising universality class.

three-peak structure is clearly discernible. This is characteristic of the 2DT regime, and indicates the vicinity of the tricritical point. In the phenomenological considerations this regime occurs only for $|r|<\exp(-\lambda D/2)/\sqrt{\overline{N}}$. We note that the distribution for that small lateral system sizes resembles at no value of ϵ the universal shape of the order parameter distribution of the 2D Ising model. We conclude that the finite-size rounding for this lateral system size sets in before we observe the crossover from 2DT to 2DI behavior, i.e., the correlation length $\xi_{\|}^{2DT\leftrightarrow 2DI}$ in Eq. (12) exceeds the lateral systems size L. For such small lateral extensions the universal properties of the transition are completely masked. Larger system sizes and a careful finite-size scaling analysis are indispensable in determining the type of transition, and accurately locate the transition temperature.

The temperature dependence of the cumulant is presented in Fig. 3(d). There is no unique intersection point, and the value of the cumulants at the crossing is larger than the universal value of the cumulant of the Ising class. This behavior indicates pronounced corrections to scaling due to the crossover from 2DT behavior away from the critical point, to 2DI behavior at the critical point. From the intersection points of neighboring system sizes and from the intersection of the cumulant with the universal value of the 2D Ising model we estimate the critical temperature to be $\epsilon_c=0.0589(10)$.

The inset of panel (d) compares the distribution of the

order parameter at our estimate of the critical temperature and the Ising scaling function. As we increase the lateral system size the ''third'' peak in the distribution vanishes, and $P(\phi)$ gradually approaches the universal scaling curve. This indicates that our largest system sizes exceed the correlation length at the crossover from 2DT to 2DI behavior. The comparison of $P(\phi)$ with the universal scaling curve for several system sizes accurately locates the critical point, and gives evidence that the transition belongs to the 2D Ising universality class. For $D \leqslant 12$ we find a single interface localization-delocalization transition of second order at $\phi = 1/2$.

2. $D=14 \approx 2R_g$: tricritical interface localization-delocalization transition

The three-peak structure in the probability distribution for $D=12$ and small lateral extensions L has indicated the vicinity of the tricritical interface localization-delocalization transition. Increasing the film thickness we need larger and larger lateral extensions to observe the 2DI behavior as $\xi_{\parallel}^{2DT \leftrightarrow 2DI}$ diverges. Right at the tricritical point the distribution of the composition is expected to exhibit a three-peak structure for all lateral system sizes, and the distribution, when scaled to unit variance and norm, coincides with a universal scaling function. Wilding and Nielaba [36] obtained this scaling function via simulations at the tricritical point of the spin-1 Blume-Capel model [37] in two dimensions. Assuming that the tricritical interface localization-delocalization transition belongs to the same universality class, we vary the film thickness D and the interaction strength ϵ as to match the probability distribution of the composition onto the predetermined scaling function of the tricritical universality class. This strategy largely facilitates the search of the tricritical interface localization-delocalization transition. Figure 4(a) displays the probability distribution of the composition for film thicknesses ranging from $D=12$ to 18 and the universal scaling curve. The temperature was adjusted for each film thickness such that the relative heights of the central and outer peaks correspond to the ratio of the universal scaling curve. For small $D<D_{\rm tri}$ the ''valley'' between the peaks is too shallow and for $D>D_{\rm tri}$ the probability between the peaks is too small. For $D \gg D_{\rm tri}$ this situation corresponds to the triple point (see below), and the probability of finding a system between the peaks is suppressed by the free energy cost of the interface between the phases with composition close to 0 or 1 and the ''soft-mode'' phase with composition $\phi=1/2$. As we increase the film thickness the temperature at which the ratio between the peak height equals 1.2 shifts toward lower temperatures and approaches the wetting transition temperature from above.

Panel (a) of Fig. 4 suggests that the tricritical transition occurs close to the film thickness $D=14$. This is further corroborated in Fig. 4(b), where we show the distribution function at $\epsilon=0.06151$ for various system sizes. Within the statistical accuracy of our data the distribution functions for the larger systems sizes collapse well onto the universal scaling curve. For smaller systems the outer peaks are slightly sharper and centered at smaller values of the order parameter. Of course, no perfect data collapse can be expected, because we can tune the film thickness only in units of the lattice spacing. In view of the statistical accuracy and possible systematic corrections to scaling, however, we did not attempt to vary the monomer-wall interaction ϵ_w as to achieve a better collapse. For $D=14$ the system is very close to the tricritical transition.

3. $D=24 \approx 3.5R_g$ and $D=48 \approx 7R_g$: critical points for $\phi \neq 1/2$

Though the system is strictly symmetric the critical points for larger film thickness ($D>D_{\rm tri}$) do not occur at $\phi=1/2$, but rather there are two critical points at critical compositions ϕ_c and $1-\phi_c$. These critical points are the finite film thickness analogs of the prewetting critical points, which occur in the limit $D \to \infty$ [17]. Below the critical temperature the phase diagram comprises two miscibility gaps. The coexisting phases correspond to surfaces with a thin and a thick enrichment layer of the preferred component. Due to the missing symmetry between the coexisting phases the coexistence value of the chemical potential $\Delta\mu_{\rm coex}$ differs from zero. We determine $\Delta\mu_{\rm coex}$ via the equal weight rule [38], i.e., we adjust $\Delta\mu$ such that

$$\int_0^{\phi^\star} d\phi\, P(\phi) \stackrel{!}{=} \int_{\phi^\star}^1 d\phi\, P(\phi) \quad \text{and} \quad \phi^\star = \int_0^1 d\phi\, P(\phi)\,\phi. \tag{18}$$

Along this coexistence curve and its finite-size extension to higher temperatures we use the cumulant intersection to locate the critical temperature. This is shown in Fig. 5(a) for the film thickness $D=24$. For the system sizes accessible in the simulations the intersection points between cumulants of neighboring systems sizes systematically shift to lower temperatures and the value of the cumulant at the intersection point gradually approaches the value of the 2D Ising universality class from above. The latter is indicated in the figure by the horizontal line. From these data we estimate the critical parameters to be $\epsilon_c=0.061(1)$, $\phi_c=0.18(2)$, and $\phi_c=0.82(2)$ respectively. This corresponds to a critical thickness $l_c=D\phi_c=0.62R_g$ of the enrichment layer. A similar procedure has been employed to locate the critical temperature in the film of thickness $D=48$. The temperature and system size dependence of the cumulants are displayed in Fig. 5(c). From this we extract the estimate $\epsilon_c=0.0625(10)$ for the critical temperature and $\phi_c=0.09(2)$ and $\phi_c=0.91(2)$ for the critical compositions. This value corresponds to a distance between the wall and the interface of $l_c=0.63R_g$. Since increasing the film thickness from $3.5R_g$ to $7R_g$ does not change T_c or l_c substantially, we are in the regime $\lambda D \gg 1$ and the critical behavior is characteristic of the prewetting critical point in the semi-infinite system.

The behavior of the cumulants and the very gradual approach of the probability distribution towards the Ising curve indicate pronounced corrections to scaling. For the simulation of the bulk phase diagram [39] a nice cumulant intersection was obtained with system sizes in the range 24^3 to 56^3. In the present study we employ systems with about an order of magnitude more polymers and obtain no clear intersection

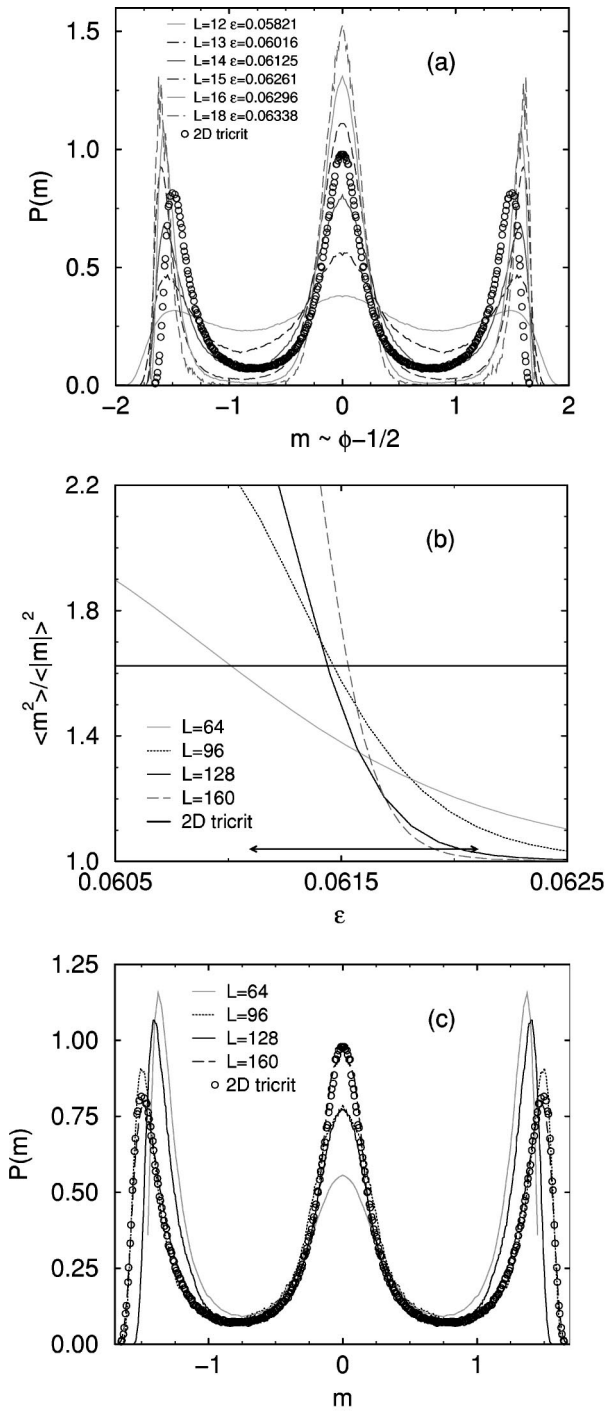

FIG. 4. (a) Probability distribution of the composition for various film thicknesses as indicated in the key. The lateral system size is $L=96$. We have adjusted the interaction strength ϵ such that the central peak is a factor 1.2 higher than the outer peaks. In accordance with convention, we have scaled the distributions to unit norm and variance. Circles mark the universal distribution of the 2D tricritical transition. (b) Temperature dependence of the cumulants for $D=14$ and lateral system sizes as indicated in the key. The horizontal line marks the cumulant value of the universal tricritical distribution. (c) Probability distribution of the composition at $\epsilon_{\rm tri}=0.06151(50)$ scaled to unit norm and variance. The universal 2D tricritical distribution (from Wilding and Nielaba [36]) is shown for comparison.

of the cumulants! There are three reasons for strong corrections to the leading 2D Ising scaling behavior: (i) The aspect ratio D/L of our simulation cell is always finite. Truly two-dimensional behavior can only be observed for a vanishing aspect ratio, and our data might fall into the broad crossover region between three- and two-dimensional critical behaviors. Such a crossover was studied in our polymer model for neutral walls [40] and walls, which attract both the same species (i.e., capillary condensation) [21]. However, we note that unlike these situations there is no three-dimensional critical point in the vicinity for antisymmetric boundary conditions. The temperature of the unmixing transition in the bulk is a factor 4 higher than the critical point in a thin film. Since the critical point in a thin film is related to the prewetting transition of the semi-infinite system, i.e., a transition with no three-dimensional analogy, we expect the corrections to be qualitatively different from the case of neutral or symmetric boundaries. (ii) Unlike the situation for small film thickness $D=12$ the probability distribution of the order parameter is asymmetric, because the critical point does not lay on the symmetry axis of the phase diagram. This missing symmetry between the two phases gives rise to field–mixing effects [34], which manifest themselves in corrections of relative order $L^{-(1-\alpha-\beta)/\nu}$. These corrections are antisymmetric to leading order and, hence, are not expected to influence even moments (like the cumulants) of the order parameter distribution profoundly. The effects are, however, detectable in the order parameter distribution which we present in Figs. 5(b) and 5(d). The distribution functions at our estimate of the critical temperature clearly lack symmetry, and very gradually approach the symmetric scaling curve of the 2D Ising universality class. (iii) Additionally, there are corrections to scaling by nonsingular background terms. One source of (noncritical) composition fluctuations are bulklike fluctuations in the *A*- and *B*-rich domains. In a bulk system, i.e., with periodic boundary conditions in all directions, the susceptibility is rather small. At $\epsilon=0.065$ it takes the value $\chi_T^{\rm bulk}=V\langle\Delta\phi^2\rangle=0.047$, with $\Delta\phi=\phi-\langle\phi\rangle$. In a system of size $96\times96\times24$ this susceptibility corresponds to composition fluctuations of the order $\sqrt{\langle\Delta\phi^2\rangle}\sim5\times10^{-4}$. Therefore, we believe that bulklike composition fluctuations are not the major source of background terms. However, we cannot rule out that the presence of an *AB* interface gives rise to enhanced composition fluctuations. Another source of corrections to scaling stems from the fluctuations in the average interface position itself. Since the effective interaction between the interface and the wall is rather weak, they give rise to a finite but large susceptibility away from the critical point. We have estimated the susceptibility from the curvature of $\ln P(\phi)$ close to the triple point (i.e., $T\approx0.9T_c$), and obtained values of the order $\chi_T\sim3\times10^2$ (and a smaller value is obtained if the interface is close to a wall.) For the same system size as above, this yields composition fluctuations of the order $\sqrt{\langle\Delta\phi^2\rangle}\sim0.04$ [a value which should be compared to $\phi_c(D=24)=0.18(2)$]. This observation partially rationalizes why the peak in the probability distribution of the composition close to $\phi=1/2$ is always broader than the peak which corresponds to the phase in which the interface is close to the wall. As we approach the critical tem-

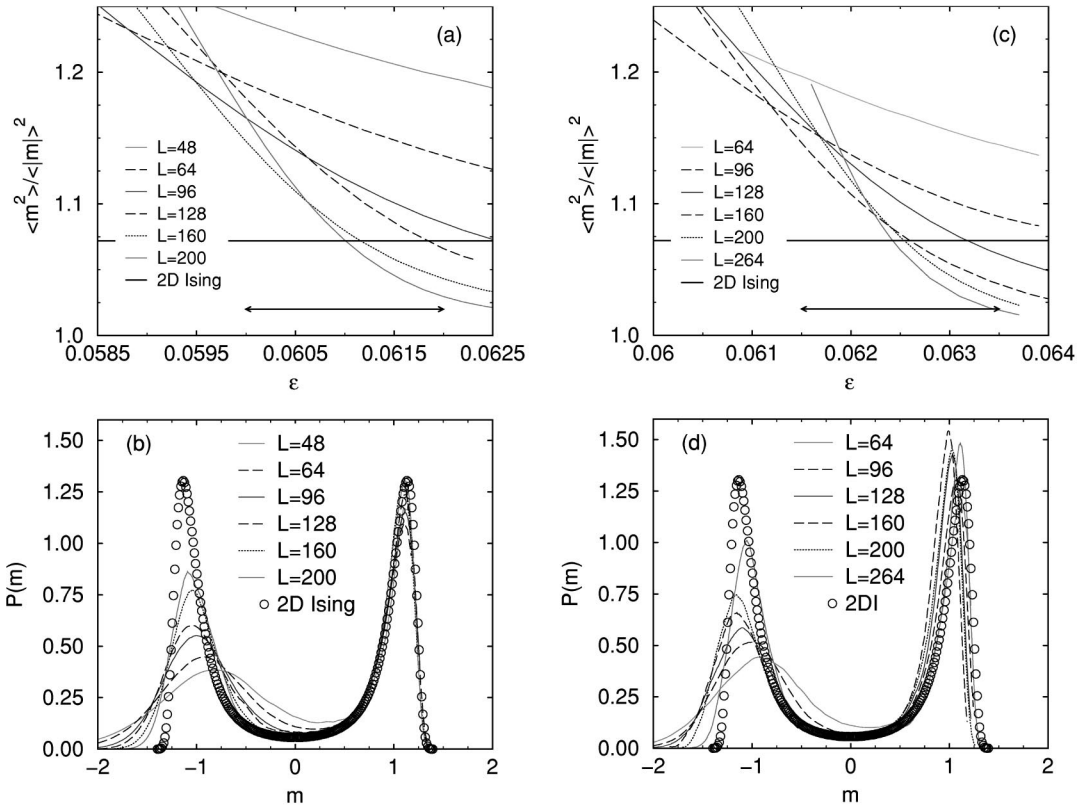

FIG. 5. (a) Temperature dependence of the cumulant $\langle m^2\rangle/\langle|m|\rangle^2$ for $D=24$ and various system sizes as indicated in the key. The arrow marks the critical temperature range $\epsilon_c=0.061(1)$. (b) Probability distribution of the composition scaled to unit norm and variance at our estimate of the critical temperature $\epsilon=0.061$. Thin lines denote the results of the Monte Carlo simulations. Histogram reweighting has been applied to extrapolate the data along the coexistence curve. Circles show the universal distribution of the 2D Ising universality class. (c) Same as (a), but for film thickness $D=48$. The inverse critical temperature is $\epsilon_c=0.0625(10)$. (d) Same as (b) but for film thickness $D=48$ and $\epsilon_c=0.0625$.

perature, composition fluctuations grow. At the critical point the typical composition fluctuations are of the order $\sqrt{\Delta\phi^2}\sim\sqrt{L^{\gamma/\nu-d}}\sim L^{-1/8}$, where we have used the critical exponents for the susceptibility $\gamma=7/4$ and the correlation length $\nu=1$ appropriate for the 2D Ising universality class. Hence for small system sizes typical fluctuations yield compositions which differ substantially from the critical composition; only for very large sizes does the composition fluctuate in the vicinity of the critical value. Moreover, the critical density is much displaced from the symmetry axis $\phi=1/2$ and typical fluctuations in a finite system are cut off by the constraint $0<\phi$ or $\phi<1$. Therefore, the susceptibility of a small system is reduced compared to the value expected from the leading scaling behavior. This observation is in accord with our Monte Carlo data, and a similar reasoning was used by Bruce and Wilding [41] in discussing background terms to the specific heat and the concomitant corrections to scaling in the energy distribution.

B. Triple point

For the largest two film thicknesses $D=24$ and 48 the interface localization-delocalization transition is first order and the concomitant two miscibility gaps join in a triple point. At this temperature an *A*-rich phase, a *B*-rich phase, and a phase where the interface is located in the middle of the film ($\phi=1/2$) coexist. The coexisting phases correspond to three peaks in the distribution of the composition. Upon increasing the lateral system size the peak positions do not shift (as opposed to the behavior at the tricritical point), the peaks become more pronounced, and configurations with intermediate compositions are more and more suppressed, because of the presence of interfaces between the coexisting phases.

The composition of the system and the average interface position are related via $l=\phi D$ (integral criterium), where we assume that the coexisting bulk phases are almost pure, i.e., $\phi_{\rm coex}^{\rm bulk}\approx 0$ or 1. From the probability distribution we then calculate the effective interface potential $g(l)$:

$$g(l)=-\frac{k_BT}{L^2}\ln P(\phi=l/D). \tag{19}$$

In principle, not only fluctuations of the interface position $\langle\Delta l^2\rangle$, but also bulklike fluctuations, contribute to composition fluctuations $\langle\Delta\phi^2\rangle\approx 1/D^2\langle\Delta l^2\rangle+(\chi_T^{\rm bulk}/L^2D)$. Since the wetting transition in a binary polymer blend occurs far below the critical point of the bulk, the bulk susceptibility is very small, and the latter contribution can be neglected.

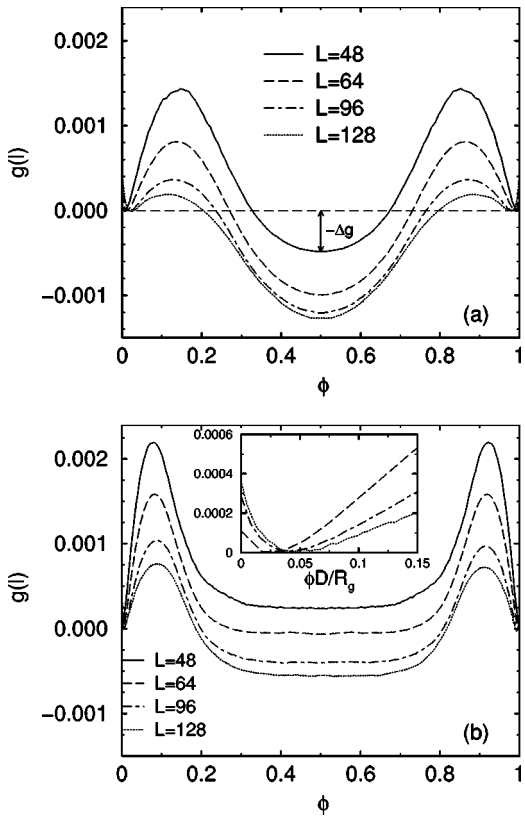

FIG. 6. (a) Dependence of the effective interface potential on the lateral system size L in a thin film of width $D=24$ at $\epsilon=0.065$. (b) same as (a), but for $D=48$ and $\epsilon=0.069$. The inset presents an enlarged view of the minimum close to the wall. The scale on the abscissa corresponds to the distance between the wall and the interface in units of R_g.

The dependence of the free energy per unit area on the position of the interface is a key ingredient into the theory of wetting [42,43,3,44–47]. The interface interacts with the boundaries and the (bare) interface potential exhibits three minima. These correspond to the three coexisting phases. In the two phases with ϕ close to 0 and 1, the interface is localized close to the wall, the interaction between the wall and the interface is rather strong, and the effective interface potential possesses a deep minimum. In the ''soft-mode'' phase the interface is only weakly bound to the center of the film, and the minimum is much broader. In Fig. 6 we present the effective interface potentials for film thicknesses $D=24$ (a) and $D=48$ (b), and various lateral system sizes in the vicinity of the triple temperature. The three minima are clearly visible; however, the shape of the interface potential and the value of the minima depend on the lateral system size L. Moreover, the minima which correspond to the localized states broaden and (slightly) shift to larger distances between the wall and interface upon increasing L (cf. the inset).

Fluctuations of the local interface position, i.e., capillary waves, lead to a renormalization of the effective interface potential $g(l)$, and cause a dependence of $g(l)$ on the lateral system size, which we observed in a microscopic model of a polymer mixture. Describing the configuration of the system only via the local position $l(x,y)$ of the interface (sharp kink approximation) we write the coarse grained free energy in form of the capillary wave Hamiltonian [44,46,48],

$$\mathcal{H}[l]=\int d^2x\left\{\frac{\sigma}{2}(\nabla l)^2+g(l)\right\}, \tag{20}$$

where σ approaches the AB interface tension between the coexisting bulk phases for large separations between the wall and the interface. An increase of σ at smaller distances l as revealed by previous MC simulations is neglected [21]. In the vicinity of a minimum of $g(l)$, we may approximate the interface potential by a parabola:

$$g(\delta l)=\text{const}+\tfrac{1}{2}\sigma k_\parallel^2\delta l^2. \tag{21}$$

δl denotes the deviation of the local interface position from the position where $g(l)$ attains its minimum. $\xi_\parallel=2\pi/k_\parallel$ is the parallel correlation length of interface fluctuations. For lateral distances much smaller than $\xi_\parallel$ the fluctuations of the local interface position are hardly perturbed by the interaction between the interface and the wall; the interface behaves like a free interface. For lateral distances which exceed $\xi_\parallel$, capillary waves are strongly suppressed. $\xi_\parallel$ is larger for the minimum of $g(l)$ in the center of the film than for the minima, in which the interface is localized at a wall. From the curvature of the effective interface potential $g(l)$ for film thickness $D=24$ we estimate $k_1=\sqrt{(d^2g/d\phi^2)/\sigma D^2}=0.26$ and $k_2=0.031$, where we have used the bulk value $\sigma=0.0382$ for the interfacial tension at $\epsilon=0.068$. For the thicker film we obtain $k_1=0.3$, but the curvature in the middle of the film could not be accurately estimated. The value is of the order $k_2\sim O(0.005)$, and we expect this value to decrease exponentially with the film thickness. Hence this fluctuation effect is the stronger the larger the film thickness. For the system sizes employed in the MC simulations, $k_\parallel L$ is of order unity.

In our Monte Carlo simulations the finite lateral system size L acts as an additional cutoff for the spectrum of interface fluctuations [14], and upon increasing L we extend the spectrum of interface fluctuations. Allowing for interface fluctuations we decrease the free energy of the system. Therefore, we expect the free energy density of the system to decrease when we increase the lateral system size, and we expect the effect to be the stronger the larger $\xi_\parallel$ is. Therefore, the free energy of the soft-mode phase becomes smaller compared to the free energy of the phase, where the interface is located close to a wall when we increase L. This effect is clearly observed in the MC simulations. To be more quantitative, we consider a system where the laterally averaged interface position is at the minimum of $g(l)$, and we expand the deviation $\delta l(x,y)$ from the minimum in a Fourier series,

$$\begin{aligned}\delta l(x,y)=\sum_{n,m=0}^{\infty}\{&a_{nm}\cos(q_nx)\cos(q_my)+b_{nm}\cos(q_nx)\\&\times\sin(q_my)+c_{nm}\sin(q_nx)\cos(q_my)\\&+d_{nm}\sin(q_nx)\sin(q_my)\},\end{aligned} \tag{22}$$

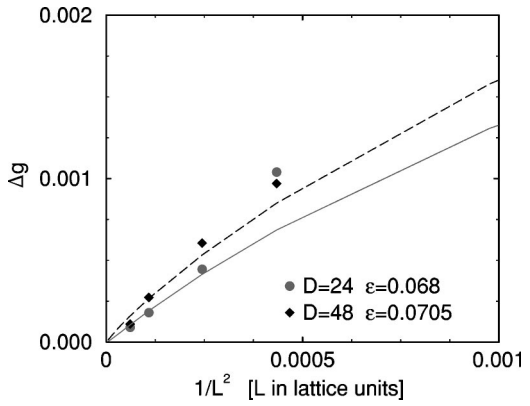

FIG. 7. Free energy difference per unit area and k_BT of the localized and delocalized state as a function of the lateral system size. The symbols represent the MC data, while the solid lines are calculated from the effective interface Hamiltonian. The temperature was chosen such that $\Delta g \to 0$ for $L \to \infty$.

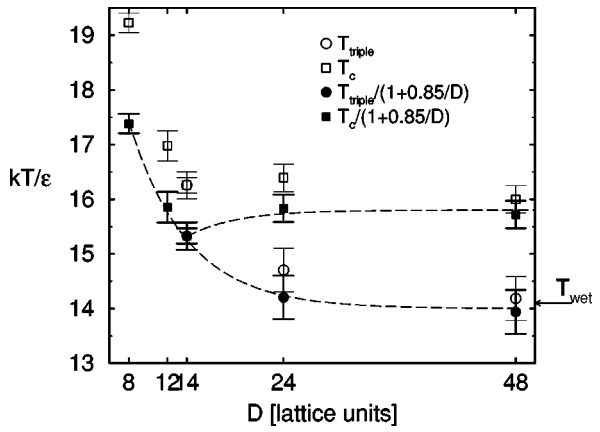

FIG. 8. Temperatures of the critical points and the triple point as a function of the film thickness D. Open symbols mark the results of the finite size scaling analysis. We have applied a correction factor $(1+0.85/D)^{-1}$ to account for the film thickness dependence of the density at the center (filled symbols). Dashed lines are only guides to the eye. The arrow on the right hand side marks the value of the wetting transition temperature obtained independently via the Young equation [21].

with $q_n = 2\pi n/L$. The coefficients $a_{00} = b_{00} = c_{00} = d_{00} = b_{0m} = c_{0m} = d_{0m} = d_{n0}$ vanish identically, and all other coefficients can take any real value. Using expansion (22) and the effective interface Hamiltonian [Eq. (20)], we calculate the average size of fluctuations,

$$\langle a_{nm}^2 \rangle = \frac{4}{\sigma (L k_\parallel)^2} \left[1 + \left(\frac{2\pi}{L k_\parallel} \right)^2 (n^2 + m^2) \right]^{-1}, \qquad (23)$$

and the free energy

$$\frac{F}{k_B T L^2} = -\frac{1}{L^2} \ln \int \mathcal{D}[l] \exp\left(\frac{-\mathcal{H}[l]}{k_B T} \right)$$

$$= \text{const} + \frac{2}{L^2} \sum_{nm=0}^{\infty} \eta_{nm} \times \ln\left\{ \frac{\sigma}{k_B T} \left[k_\parallel^2 + \left(\frac{2\pi}{L} \right)^2 (n^2 + m^2) \right] \right\}, \qquad (24)$$

where the factor η_{nm} takes the values $\eta_{00} = 0$, $\eta_{n0} = \eta_{0m} = 1/2$, and $\eta_{nm} = 1$ for $n \neq 0$ and $m \neq 0$ in order to account for the restriction on the coefficients a, b, c, and d. The additive constant is independent of the wave vector cutoff $k_\parallel$. The dependence of the free energy on the system size is dominated by the small q behavior. In this regime the discrete nature of the wave vector space matters and, hence, we do not replace the sum over q by integrals. Using the measured values of the wave vector cutoffs, we calculate the lateral system size dependence of the free energy difference between the soft-mode phase and the delocalized state. The results are compared to the MC data in Fig. 7. Good agreement is found for large L, whereas there are deviations for smaller L. For small L the amplitude of the fluctuations becomes large, and the parabolic interface potential is no longer a good approximation—especially for the localized state where the interface is located very close to the walls. We have used histogram extrapolation to adjust the temperature such that the difference $\Delta g(l) = g_2 - g_1$ of the minima vanishes. This corresponds to the equal height criterium for the triple point. The equal weight condition, which we have applied to determine the binodals close to the critical points, would require $\Delta g = (1/L^2) \ln(k_1/k_2)$. Both conditions agree, of course, when we extrapolate our results to $L \to \infty$. From this procedure we obtain the following estimates for the triple point: $1/\epsilon_{\text{triple}} = 14.7(4)$ and $\phi_{\text{triple}} = 0.015$, 0.5, 0.985 for $D = 24$ and $1/\epsilon_t = 14.2(4)$ and $\phi_{\text{triple}} = 0.0066$, 0.5, 0.9934 for $D = 48$. The thickness of the microscopic enrichment layer at the wetting transition temperature is of the order $l_{\text{wet}} = 0.05 R_g$, a value which is consistent with expectation for strong first order wetting transitions.

The dependence of the critical temperature and the triple temperature on the film thickness is summarized in Fig. 8. When we increase the film thickness the critical temperature $1/\epsilon_c$ shows a non-monotonic dependence. At $D = 14$ the tricritical point (where the critical temperature and the triple temperature merge) occurs at $\epsilon_{\text{tri}} = 0.0615(5)$; at film thickness $D = 24$ we find $\epsilon_c = 0.0610(10)$, and at $D = 48$ $\epsilon_c = 0.0625(10)$. This effect is rooted in two opposing effects. On the one hand, self-consistent-field (SCF) calculations predict the Flory-Huggins parameter $\chi_c^{\text{SCF}}(D)$ to decrease upon increasing the film thickness D for an incompressible fluid. This shift in temperature decreases exponentially with the film thickness. One the other hand, packing effects, which are not incorporated in the self-consistent-field calculations, increase the density in the bulklike portion of the film when we decrease the film thickness. These packing effects at the walls depend strongly on the computational model, but qualitatively similar effects might occur in experimental systems as well. This thickness dependence of the density in the middle of the film modifies the relation between the depth of the square well potential and the χ parameter. This leads to a behavior of the form $\epsilon_c \sim \chi_c^{\text{SCF}}/(1 + 0.85/D)$, where we use the dependence of the density profile (cf. Fig. 2) on the film thickness as obtained by direct measurement in the Monte

Carlo simulations. A dependence of the fluid packing structure on the density is neglected. A similar $1/D$ correction to the difference in surface free energies between the A- and B-rich phases was observed in previous simulations [21]. Attempting to separate these two effects we also present $[(1+0.85/D)\epsilon_c]^{-1}$, which corresponds to the inverse Flory-Huggins parameter. Within the error bars the behavior of this quantity is consistent with the mean field prediction. The critical value of the inverse Flory-Huggins parameter increases, and the triple value decreases as we increase the film thickness. The latter approaches the wetting transition temperature [21] $T_{\mathrm{wet}}=14.1(7)$ from above.

C. Phase diagram

For a film thickness $D=48$ we have determined the complete phase diagram. Close to the critical point we assume a 2DI behavior, with an exponent $\beta=1/8$ for the order parameter, and employ finite-size scaling to estimate the critical amplitude. Outside the critical region but above the triple temperature, we have estimated the location of the binodals via the equal weight criterium in a system of size $L=64$, but no finite-size analysis has been applied. The phase diagram for a blend confined into a film with antisymmetric walls is presented in Fig. 9. Figure 9(a) shows that confinement into a film with antisymmetric boundary conditions enlarges the one phase region up to the prewetting critical temperature. Since the wetting transition in binary polymer blends occurs far below the unmixing critical temperature in the bulk, the effect is quite pronounced. The temperature region between the prewetting critical point and the triple point is about 11% of the wetting transition temperature. This value strongly depends on the details of the structure at the walls. The stronger the wetting transition, the larger the prewetting lines and the more extended the region of the two miscibility gaps. The phase diagram of the bulk and a film with symmetric walls are displayed for comparison in Fig. 9. The symmetric film, has the same thickness as the antisymmetric film, and the monomer-wall interactions at one wall are identical and attract the A component. While the prewetting at the wall which ''prefers'' the A component leads to a two phase region in the antisymmetric case, there is only a change in curvature of the binodal detectable in the symmetric case.

Panel (b) of Fig. 9 presents the phase diagram as a function of temperature and exchange chemical potential. In the antisymmetric case $\Delta\mu_{\mathrm{coex}}=0$ up to the triple temperature. There, two coexistence lines emerge which are the thin film analogies of the prewetting lines at the two walls. Since the monomer-wall interactions are short ranged, the prewetting line in the bulk and the coexistence curves in the film deviate from the bulk coexistence value linearly (up to logarithmic corrections) [49]. They end in two critical points. Though the system is strictly symmetric with respect to exchanging $A\rightleftharpoons B$, phase coexistence is not restricted to $\Delta\mu=0$, and the coexisting phases are not related by the symmetry of the Hamiltonian. The coexistence curve of the symmetric film is shown for comparison. The coexistence value of the chemical potential is shifted to values disfavoring the component attracted by both walls. There is a change in the temperature

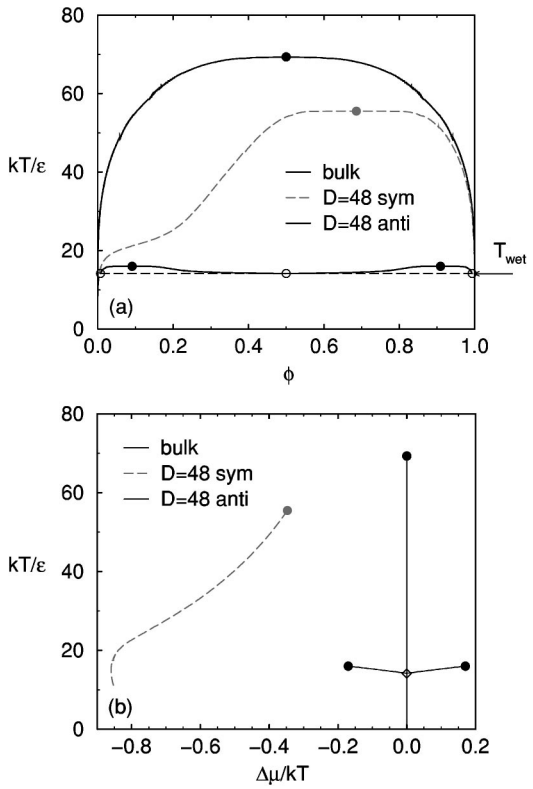

FIG. 9. (a) Phase diagram of a binary polymer blend ($N=32$). The upper curve shows the binodals in the infinite system; the middle one corresponds to a thin film of thickness $D=48$ and symmetric boundary fields $\epsilon_w=0.16$, which both ''prefer'' species A. The lower curve corresponds to a thin film with antisymmetric surfaces. The arrow marks the location of the wetting transition. Full circles mark critical points; open circles and dashed line denote the triple point. (b) Coexistence curves in the $(T,\Delta\mu)$ plane. Circles mark critical points, and the diamond indicates the location of the wetting transition temperature. This is indistinguishable from the temperature of the triple point.

dependence of the coexistence curve close to the wetting transition temperature, but the coexistence curve stays far away from the prewetting line. If the two lines were to intersect there would also be a triple point in the symmetric case [21,50]. Since the shift of the chemical potential $\Delta\mu$ is roughly proportional to the inverse film thickness (Kelvin equation), we expect a triple point to occur only for much larger film thicknesses. This is in accord with self-consistent-field calculations [21]. The typical distance l between the interface and the wall at coexistence is of order $D/2$ in the antisymmetric case, while it is only of the order $R_g \ln D/R_g$ in the symmetric case. Hence smaller film thicknesses are sufficient to study the interaction between the interface and the wall, and antisymmetric boundary conditions are computationally more efficient to investigate the wetting behavior.

V. SUMMARY AND DISCUSSION

We have studied the phase diagram of a symmetric polymer mixture in a thin film with antisymmetric boundary conditions via large scale Monte Carlo simulations. The walls interact with monomers via a short range potential; one wall

attracts the *A* component and repels the *B* component, while the interaction at the opposite wall is exactly reversed. The salient features of the phase diagram and its dependence on the film thickness, as obtained by our MC simulations, are in accord with the results of mean field theory [9,17,18]. Fluctuations, which are neglected in the mean field calculations, do not modify the qualitative phase behavior. However, they give rise to a rich crossover behavior between the Ising critical behavior, the tricritical behavior, and their mean field counterparts. This has been elucidated by phenomenological considerations, and is qualitatively consistent with our simulation results.

Since the critical point of the thin binary polymer film occurs at a much lower temperature than the unmixing transition in the bulk, bulklike composition fluctuations are only of minor importance. The dominant fluctuations of the composition of the film arise from capillary waves at the interface between the *A*- and *B*-rich regions in the film. The interaction between the walls, and the interface is rather small, because it is mediated via the distortion of the interface profiles at the walls and the strength of the interaction decreases exponentially with the distance. Hence the interface is only very weakly bound to the minimum of the effective interface potential. These large fluctuations give rise to rather pronounced corrections to scaling in our systems of limited size. However, using the cumulant intersection method [35] and the matching of the order parameter distribution onto the predetermined universal scaling function [34], we give evidence of the 2D Ising universal character of the critical points. The same strategy has proven computationally very convenient to locate the tricritical point as a function of the film thickness [36]. This technique allows us to locate the critical points of the confined complex fluid mixture with an accuracy of a few percent.

Interface fluctuation do not only impart 2D Ising critical behavior onto the critical points, but they are important in the whole temperature range. Monitoring the probability distribution of the laterally averaged interface position, we extract the effective interface potential $g(l)$. Its dependence on the lateral system size yields direct evidence of the renormalization of the interface potential by interface fluctuations. Interface fluctuations lead to a broadening of the minima in the interface potential, a shift of the minima toward the center of the film, and a relative reduction of the free energy of the broader minimum. This leads to a systematic overestimation of the triple temperature by the mean field calculations.

Moreover, our simulations indicate that packing effects in thin films result in corrections of the order $1/D$ to the density of the film or to the effective Flory-Huggins parameter. Such corrections are likely to mask completely the subtle thickness dependence of the triple temperature and the triple temperature predicted by the mean field calculations. For short range interactions between walls and monomers the predicted shifts decrease exponentially with the film thickness *D*. However, power-law dependencies are expected for the case of long range (i.e., van der Waals) interactions between walls and monomers.

The gross features of the phase diagram, as well as our simulation and analysis techniques, are not restricted to binary polymer fluids, but generally apply to binary liquid mixtures in confined geometries. Moreover, mean field calculations [17] indicate that for small deviations from perfectly antisymmetric boundary conditions a qualitatively similar phase behavior emerges. The stronger the first order wetting transitions at the boundaries, the larger the deviations from antisymmetry permissible without alternating the topology of the phase diagram. Hence a thin binary film on a substrate against air and/or vacuum, where the substrate energetically favors one component of the mixture while the other component has an affinity to the air surface, is an experimental realization of the boundary conditions discussed here. Our findings also imply that ultrathin enrichment layers at one surface are unstable in the temperature range $T_{\mathrm{wet}} < T < T_c$. Such effects were observed experimentally [51] in polymeric films, although for a liquid-vapor transition instead of a liquid-liquid demixing. However, recent experiments have observed the wetting transition in binary polymer blends [52,53].

ACKNOWLEDGMENTS

It is a great pleasure to thank N. B. Wilding for stimulating discussions and for providing the universal probability distributions of the order parameter at the 2D Ising critical point and 2D tricritical point. We have also benefited from discussions with E. V. Albano and A. De Virgiliis. Financial support by the DFG under Grant No. Bi 314/17 in the priority program ''wetting and structure formation at interfaces'' and the DAAD/PROALAR2000, as well as generous grants of computing time at the NIC Jülich, the HLR Stuttgart, and the computing center in Mainz, are gratefully acknowledged.

[1] R. Evans, J. Phys.: Condens. Matter **2**, 8989 (1990).
[2] A. O. Parry, J. Phys.: Condens. Matter **8**, 10 761 (1996).
[3] S. Dietrich, in *Phase Transitions and Critical Phenomena*, edited by C. Domb and J. Lebowitz (Academic Press, London, 1988), Vol. 12.
[4] P. G. de Gennes, Rev. Mod. Phys. **57**, 827 (1985).
[5] A. Budkowski, Adv. Polym. Sci. **148**, 1 (1999); K. Binder, *ibid.* **138**, 1 (1999).
[6] M. E. Fisher and H. Nakanishi, J. Chem. Phys. **75**, 5857 (1981); H. Nakanishi and M. E. Fisher, *ibid.* **78**, 3279 (1983).
[7] F. Brochard-Wyart and P.-G. de Gennes, Acad. Sci., Paris **297**, 223 (1983).
[8] A. O. Parry and R. Evans, Phys. Rev. Lett. **64**, 439 (1990); Physica A **181**, 250 (1992).
[9] M. R. Swift, A. L. Owczarek, and J. O. Indekeu, Europhys. Lett. **14**, 475 (1991).
[10] K. Binder, D. P. Landau, and A. M. Ferrenberg, Phys. Rev. Lett. **74**, 298 (1995); Phys. Rev. E **51**, 2823 (1995); E. V. Albano, K. Binder, D. W. Heermann, and W. Paul, Surf. Sci. **233**, 151 (1989).

[11] J. O. Indekeu, A. L. Owczarek, and M. R. Swift, Phys. Rev. Lett. **66**, 2174 (1991); A. O. Parry and R. Evans, *ibid.* **66**, 2175 (1991).
[12] J. Rogiers and J. O. Indekeu, Europhys. Lett. **24**, 21 (1993); E. Carlon and A. Drzewinski, Phys. Rev. Lett. **79**, 1591 (1997).
[13] K. Binder, R. Evans, D. P. Landau, and A. M. Ferrenberg, Phys. Rev. E **53**, 5023 (1996).
[14] A. Werner, F. Schmid, M. Müller, and K. Binder, J. Chem. Phys. **107**, 8175 (1997).
[15] T. Kerle, J. Klein, and K. Binder, Phys. Rev. Lett. **77**, 1318 (1996); Eur. Phys. J. B **7**, 401 (1999).
[16] M. Sferrazza, M. Heppenstall-Butler, R. Cubitt, D. Bucknall, J. Webster, and R. A. L. Jones, Phys. Rev. Lett. **81**, 5173 (1998); M. Sferrazza, C. Xiao, R. A. L. Jones, D. G. Bucknall, J. Webster, and J. Penfold, *ibid.* **78**, 3693 (1997).
[17] M. Müller, K. Binder, and E. V. Albano, Europhys. Lett. **49**, 724 (2000).
[18] M. Müller, K. Binder, and E. V. Albano, Physica A **279**, 188 (2000); M. Müller, E. V. Albano, and K. Binder, Phys. Rev. E **62**, 5281 (2000).
[19] A. M. Ferrenberg, D. P. Landau, and K. Binder, Phys. Rev. E **58**, 3353 (1998).
[20] M. Müller, Macromol. Theory Simul. **8**, 343 (1999).
[21] M. Müller and K. Binder, Macromolecules **31**, 8323 (1998).
[22] B. Nienhuis, A. N. Berker, E. K. Riedel, and M. Schick, Phys. Rev. Lett. **43**, 737 (1979).
[23] M. P. M. den Nijs, J. Phys. A **12**, 1857 (1979).
[24] R. B. Pearson, Phys. Rev. B **22**, 2579 (1980).
[25] V. L. Ginzburg, Fiz. Tverd. Tela (Leningrad) **2**, 2031 (1960) [Sov. Phys. Solid State **1**, 1824 (1960)]; P. G. de Gennes, J. Phys. (France) Lett. **38**, L-441 (1977); J. F. Joanny, J. Phys. A **11**, L-117 (1978); K. Binder, Phys. Rev. A **29**, 341 (1984).
[26] I. Carmesin and K. Kremer, Macromolecules **21**, 2819 (1988).
[27] H.-P. Deutsch and K. Binder, J. Chem. Phys. **94**, 2294 (1991).
[28] J. Baschnagel *et al.*, Adv. Polym. Sci. **152**, 41 (2000); V. Tries, W. Paul, J. Baschnagel, and K. Binder, J. Chem. Phys. **106**, 738 (1997).
[29] M. Müller, K. Binder, and W. Oed, J. Chem. Soc., Faraday Trans. **91**, 2369 (1995).
[30] M. Müller and K. Binder, Macromolecules **28**, 1825 (1995).
[31] A. Sariban and K. Binder, J. Chem. Phys. **86**, 5859 (1987).
[32] B. A. Berg and T. Neuhaus, Phys. Rev. Lett. **68**, 9 (1992); J. Lee, *ibid.* **71**, 211 (1993); E. Marinari and G. Parisi, Europhys. Lett. **19**, 451 (1992).
[33] A. M. Ferrenberg and R. H. Swendsen, Phys. Rev. Lett. **61**, 2635 (1988); **63**, 1195 (1989); A. Bennett, J. Comput. Phys. **22**, 245 (1972).
[34] A. D. Bruce and N. B. Wilding, Phys. Rev. Lett. **68**, 193 (1992); N. B. Wilding, Phys. Rev. E **52**, 602 (1995).
[35] K. Binder, Z. Phys. B: Condens. Matter **43**, 119 (1981); Phys. Rev. Lett. **47**, 693 (1981); Rep. Prog. Phys. **60**, 487 (1997).
[36] N. B. Wilding and P. Nielaba, Phys. Rev. E **53**, 926 (1996).
[37] M. Blume, Phys. Rev. **141**, 517 (1966); H. W. Capel, Physica (Amsterdam) **32**, 966 (1966).
[38] C. Borgs and R. Kotecky, J. Stat. Phys. **61**, 79 (1990); Phys. Rev. Lett. **68**, 1734 (1992).
[39] H.-P. Deutsch and K. Binder, Macromolecules **25**, 6214 (1992).
[40] Y. Rouault, J. Baschnagel, and K. Binder, J. Stat. Phys. **80**, 1009 (1995).
[41] A. D. Bruce and N. B. Wilding, Phys. Rev. E **60**, 3748 (1999).
[42] J. W. Cahn, J. Chem. Phys. **66**, 3667 (1977).
[43] M. Schick, in *Liquids at Interfaces, Les Houches, Session XLVIII*, edited by J. Charvolin, J. F. Joanny, and J. Zinn-Justin (Elsevier, Amsterdam, 1990).
[44] R. Lipowsky, D. M. Kroll, and R. K. P. Zia, Phys. Rev. B **27**, 4499 (1983).
[45] E. Brezin, B. I. Halperin, and S. Leibler, Phys. Rev. Lett. **50**, 1387 (1983).
[46] D. S. Fisher and D. A. Huse, Phys. Rev. B **32**, 247 (1985).
[47] M. E. Fisher and H. Wen, Phys. Rev. Lett. **68**, 3654 (1992).
[48] D. A. Huse, W. van Saarloos, and J. D. Weeks, Phys. Rev. B **32**, 233 (1985).
[49] E. H. Hauge and M. Schick, Phys. Rev. B **27**, 4288 (1983).
[50] D. Nicolaides and R. Evans, Phys. Rev. B **39**, 9336 (1989); R. Evans and U. Marini Bettolo Marconi, Phys. Rev. A **32**, 3817 (1985).
[51] W. Zhao, M. H. Rafailovich, J. Sokolov, L. J. Fetters, R. Plano, M. K. Sanyal, S. K. Sinha, and B. B. Sauer, Phys. Rev. Lett. **70**, 1453 (1993).
[52] J. Rysz, A. Budkowski, A. Bernasik, J. Klein, K. Kowalski, J. Jedlinski, and L. J. Fetters, Europhys. Lett. **50**, 35 (2000).
[53] M. Geoghegan, H. Ermer, G. Jüngst, G. Krausch, and R. Brenn, Phys. Rev. E **62**, 940 (2000).